Journal of Alloys and Compounds 509 (2011) 782–788

Contents lists available at ScienceDirect

Journal of Alloys and Compounds

journal homepage: www.elsevier.com/locate/jallcom

Optimization of the pulsed current gas tungsten arc welding (PCGTAW) parameters for corrosion resistance of super duplex stainless steel (UNS S32760) welds using the Taguchi method

M. Yousefieh [1], M. Shamanian *, A. Saatchi

Department of Materials Engineering, Isfahan University of Technology, Isfahan 84156-83111, Iran

ARTICLE INFO

Article history:
Received 29 May 2010
Received in revised form
14 September 2010
Accepted 17 September 2010
Available online 24 September 2010

Keywords:
Pulse current gas tungsten arc welding
Super duplex stainless steel
Corrosion
Taguchi method
Analysis of variance

ABSTRACT

In the present work, a design of experiment (DOE) technique, the Taguchi method, has been used to optimize the pulsed current gas tungsten arc welding (PCGTAW) parameters for the corrosion resistance of super duplex stainless steel (UNS S32760) welds. A L_9 (3^4) orthogonal array (OA) of Taguchi design which involves nine experiments for four parameters (pulse current, background current, % on time, pulse frequency) with three levels was used. Corrosion resistance in 3.5%NaCl solution was evaluated by anodic polarization tests at room temperature. Analysis of variance (ANOVA) is performed on the measured data and S/N (signal to noise) ratios. The higher the better response category was selected to obtain optimum conditions. The optimum conditions providing the highest pitting potential were estimated. The optimum conditions were found as the second level of pulse current (120 A), second level of background current (60 A), third level of % on time (80) and third level of pulse frequency (5 Hz). Under these conditions, pitting potential was predicted as 1.04 V_{SCE} that was very close to the observed value of 1.06 V_{SCE}. As a result of Taguchi analysis in this study, the pulse current was the most influencing parameter on the corrosion resistance and the background current had the next most significant effect. The percentage contributions of pulse current, background current, % on time, and pulse frequency to the corrosion resistance are 66.28%, 25.97%, 2.71% and 5.04%, respectively. Consequently, the Taguchi method was found to be promising technique to obtain the optimum conditions for such studies. Moreover, the experimental results obtained confirm the adequacy and effectiveness of this approach.

1. Introduction

Super duplex stainless steels (SDSS), with a microstructure included of nearly equal proportions of ferrite (α) and austenite (γ), have found widespread use in industries such as oil and gas, petrochemical and chemical processing. Their popularity is attributed to an attractive combination of high corrosion resistance, excellent mechanical properties, good weldability and also a relatively low cost compared to other higher performance materials, such as super austenitic stainless steels and Ni-based alloys. During welding and subsequently, several transformations take place in the heat-affected zone and in the weld metal. The best general properties of SDSS is obtained when the ferrite-austenite ratio is close to 50:50 [1], and other phases, such as Cr_2N, ε (Cu), sigma and chi, are not present. Nucleation and growth of deleterious phases have been studied by many authors [2–7].

Historically, in welding operations the great difficulty is to obtain austenite amounts close to 50% and to avoid the formation of deleterious phases such as sigma and Cr_2N on cooling and reheating passes. In fact, very low heat inputs lead to high ferrite contents and intense chromium nitride precipitation. On the other hand, high heat inputs and/or long exposure to temperatures in the 600–1000 °C range may cause precipitation of brittle intermetallic phases such as σ or χ [8]. In general, welding specifications must be designed to obtain phase proportions (ferrite/austenite ratio) near 1:1 and to avoid σ and Cr_2N precipitation by controlling and limiting the heat input to 0.5–2.0 kJ/mm [9].

Pulsed current gas tungsten arc welding (PCGTAW), developed in the 1950s, is a variation of constant current gas tungsten arc welding (CCGTAW) which involves cycling of the welding current from a high level to a low level at a selected regular frequency. The high level of the pulse current is generally selected to give adequate penetration and bead contour, while the low level of the background current is set at a level sufficient to maintain a stable arc. This permits arc energy to be used efficiently to fuse a spot

* Corresponding author. Tel.: +98 311 3915737; fax: +98 311 3915737.
E-mail addresses: m.yousefieh@ma.iut.ac.ir (M. Yousefieh), shamanian@cc.iut.ac.ir (M. Shamanian).
[1] Tel.: +98 912 431 0994.

0925-8388/$ – see front matter © 2010 Elsevier B.V. All rights reserved.
doi:10.1016/j.jallcom.2010.09.087

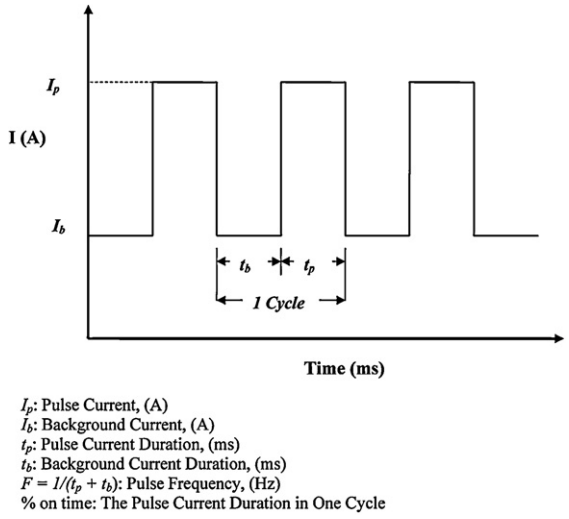

Fig. 1. Defined pulse and background current modes.

of controlled dimensions in a short time producing the weld as a series of overlapping nuggets and limits the wastage of heat by conduction into the adjacent parent material as in normal constant current welding. In contrast to constant current welding, the fact that the heat energy required to melt the base material is supplied only during peak current pulses for brief intervals of time allows the heat to dissipate into the base material leading to a narrower heat affected zone (HAZ). The technique has secured a niche for itself in specific applications such as in welding of root passes of tubes, and in welding thin sheets, where precise control over penetration and heat input are required to avoid burn through [10]. The PCGTAW has many specific advantages compared to CCGTAW, such as enhanced arc stability, increased weld depth to width ratio, refined grain size, reduced porosity, low distortion, reduction in the heat-affected zone (HAZ) and better control of heat input [11]. In general, the pulsed current GTAW process is suitable for joining thin and medium thickness materials, e.g. stainless steel sheets, and for applications where metallurgical control of the weld metal is critical [12]. All these advantages will help in improving mechanical and corrosion properties. The definitions of pulse current, background current and time duration modes are schematically illustrated in Fig. 1.

Reported research work related to the effect of pulsed current parameters on corrosion and metallurgical properties are very scanty. Moreover, no systematic study has been reported so far to analyze the influence of pulsed current parameters on corrosion and metallurgical properties.

Taguchi method is a systematic approach to design and analyze experiments for improving the quality characteristics. Various steps of Taguchi method are shown in Fig. 2 [13].

This study will be useful to select suitable welding process variables and their values to control the heat input and cooling rates during welding such that the corrosion resistance of the weld could be improved. The purpose of the present investigation is to optimize the pulsed GTAW process parameters for increasing the corrosion properties of super duplex UNS S32760 stainless steel welds using Taguchi method.

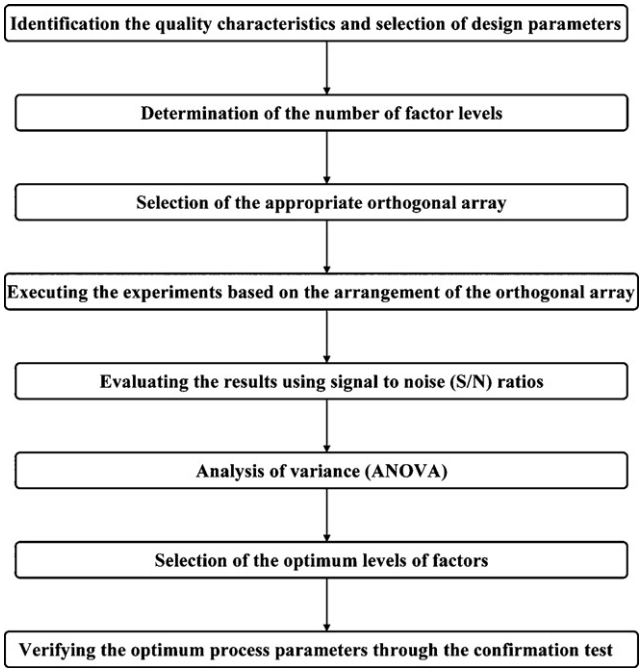

Fig. 2. Several steps of Taguchi method.

2. Experimental procedures

The material chosen for the investigation was a 5 mm thick, 500 mm diameter SDSS pipe corresponding to UNS S32760, whose composition is given in Table 1. Welding was performed using pulsed current GTAW (PCGTAW). High purity argon was used as arc plasma and shielding gas with a flow rate 10 l/min.

In CCGTAW process, heat input is calculated from constant current, whereas in the PCGTAW process, heat input is calculated from the mean current (I_m). The equation for mean current [12] may be written as:

$$I_m = \frac{I_p \times t_p + I_b \times t_b}{t_p + t_b} \text{ amps} \quad (1)$$

Heat input (HI) is calculated using following equation [12]:

$$HI = \eta \times \frac{I_m \times V}{S} \text{ (kJ/mm)} \quad (2)$$

I_p pulse current, amps; I_b background current, amps; t_b background current duration, ms; t_p pulse current duration, ms; S welding speed, cm/min; V voltage, V; η efficiency of the welding process; For the PCGTAW process, arc efficiency is taken as 60% [12].

Volumetric fractions of austenite and ferrite in the as received materials, and deleterious phases in samples, were determined by quantitative metallography using Image Tool software [14]. The samples were prepared by grinding, polishing and etching by following procedure:

Electrolytic etching in a KOH solution (100 ml H_2O + 15 g of potassium hydroxide), applying 3 V for 12 s. The parameters of this reagent were adjusted to reveal clearly σ phase and other deleterious phases, such as χ, γ_2, and eventually Cr_2N that precipitated in association with σ [15–17]. A number of samples were electrolytically etched by using 10% oxalic acid solution (8 V, 50 s) to reveal Cr_2N in the ferrite.

The microstructures of samples were observed by scanning electron microscope (SEM) equipped with energy dispersive X-ray spectrometer (EDX) system. The X-ray count rate was estimated as 2×10^3 counts per second (cps).

Anodic polarization tests were conducted at room temperature using a potentiostat–galvanostat EG&G-263 A. The tests were conducted in a conventional three-electrode cell, with Pt foil as the auxiliary electrode, and a saturated calomel electrode (SCE) as the reference electrode. The working electrode was constructed using the SDSS samples embedded in epoxy resin, with a copper wire providing electrical contact. The tests were initiated after nearly steady-state open circuit potential

Table 1
Chemical composition of the base and filler materials (wt.%).

Element	C	Mn	P	S	Si	Cr	Ni	Mo	N	Cu
Base metal (UNS S32760)	0.03	0.82	0.02	0.01	0.93	25.7	6.3	3.4	0.23	0.61
Filler metal (ER 2594)	0.03	0.73	0.001	0.002	0.94	25.9	9.2	4.2	0.22	0.54

Table 2
Parameters and their values corresponding to their levels studied in experiments (Voltage = 15 V, Travel speed = 10 cm/min).

Parameters	Designation	Levels		
		1	2	3
Pulse current (A)	A	100	120	140
Background current (A)	B	50	60	70
% On time	C	40	60	80
Pulse frequency (Hz)	D	1	3	5

Table 3
A design of L_9 (3^4) by the Taguchi method.

Trial no.	Factors			
	A	B	C	D
1	1	1	1	1
2	1	2	2	2
3	1	3	3	3
4	2	1	2	3
5	2	2	3	1
6	2	3	1	2
7	3	1	3	2
8	3	2	1	3
9	3	3	2	1

(Eoc) had developed (about 30 min). After that, a potential sweep was applied in the anodic direction at 1 mV s^{-1} until a current density of 1 mA/cm^2 was reached. Prior to each experiment, the working electrodes were ground and polished with 0.1 μm alumina paste, degreased with alcohol and cleaned in water. The edges of the samples were protected to avoid crevice corrosion. The working solution was 3.5% NaCl. The corrosion behavior was evaluated by the absolute value of the pitting potential (E_{pit}). At a fixed temperature, the higher the pitting potential in anodic polarization test the higher the pitting resistance [17].

3. Experimental design based on Taguchi method

Four factors (pulse current, background current, % on time, pulse frequency) with three levels were selected, as shown in Table 2. The total degrees of freedom need to be computed to select an appropriate orthogonal array. Basically the degrees of freedom for the orthogonal array should be greater than or at least equal to those for the parameters [13]. For example, a four level design parameter counts for three degrees of freedom (DOF). In this study, there are eight degrees of freedom owing to being four factors. L_9 (3^4) orthogonal array of Taguchi design which involves nine experiments for four parameters with three levels was used. This array has eight DOF. Experimental plan table according to L_9 (3^4) is shown in Table 3 [18]. The order of the experiments was made random in order to avoid noise sources.

With the selection of L9 (3^4) orthogonal array, the number of experiments required can be reduced to 9. So, 9 experiments should be conducted in order to study the main effects and interactions whereas full factorial experimentation would require $3^4 = 81$ number of experiments.

Taguchi method recommends the S/N ratio (signal-to-noise), which is a performance characteristic, instead of the average value. Optimum conditions were determined using the S/N ratio of experimental results [19]. There are three categories of performance characteristics, the higher the better (HB), lower the better (LB) and the nominal the better (NB). The larger S/N ratio respects to better performance characteristic. In the present study, corrosion resistances are treated as a characteristic value. Since the corrosion resistance welds intended to be maximized, the S/N ratio for HB characteristics was selected, which can be calculated as following equation [19]:

$$\frac{S}{N} = -10\log_{10}\left(\frac{1}{n}\sum_{i=1}^{n}\frac{1}{Y_i^2}\right) \quad (3)$$

where S/N are performance statistics, defined as the signal to noise ratio (S/N unit: dB), n the number of repetitions for an experimental combination, and Y_i a performance value of the ith experiment.

Then the mean S/N ratios at each level for various factors must be calculated. Moreover, the optimal level, that is the largest S/N ratio among all levels of the factors, can be determined.

Finally, confirmation experiment must be carried out with optimal process parameters to verify predicted results. If the predicted results are confirmed, the suggested optimum working conditions will be adopted [13].

4. Results and discussion

4.1. Taguchi results

The calculation of the corrosion resistances of samples are based on the pitting potentials (E_{pit}) which were derived from the anodic polarization curves. The measured pitting potentials and the computed S/N ratios and heat inputs for each series of experiments are presented in Table 4. The response of each factor to its individual level was calculated by averaging the S/N ratios of all experiments at each level for each factor. In order to evaluate the influence of each factor on the corrosion resistance, the S/N ratio for each factor should be computed. The S/N ratio for a single factor can be calculated by averaging the value of S/N ratios at different levels. For example, the mean S/N ratio for background current at level 1 can be calculated by averaging the S/N ratios for the experiments 1, 4 and 7. The mean S/N ratio for every factor at different levels is calculated similarly. The determined factor responses are summarized in Table 5.

Figs. 3–6 show the effect of the four factors, pulse current, background current, % on time and pulse frequency, on the mean S/N ratios, respectively. As seen from figures, overall mean value was calculated as −0.515934 from all Taguchi experiment results. Also it can be seen that the slopes of the lines between different levels are not the same for pulse current, background current and pulse frequency factors. So, the levels have different influence on corrosion resistance. Furthermore, Figs. 3–6 suggest that pulse current and

Table 4
Experimental results for pitting potential and corresponding S/N ratios and heat inputs.

Trial no.	Pulse current (A)	Background current (A)	% On time	Pulse frequency (Hz)	E_{pit} (V_{SCE})	S/N ratio (dB)	Heat input (kJ/mm)
1	100	50	40	1	0.88	−1.11035	0.630
2	100	60	60	3	0.92	−0.72424	0.763
3	100	70	80	5	0.94	−0.53744	0.846
4	120	50	80	3	0.97	−0.26457	0.955
5	120	60	40	5	1.03	0.25674	0.756
6	120	70	60	1	0.98	−0.17548	0.900
7	140	50	60	5	0.89	−1.01220	0.936
8	140	60	80	1	0.95	−0.44553	1.116
9	140	70	40	3	0.93	−0.63034	0.890

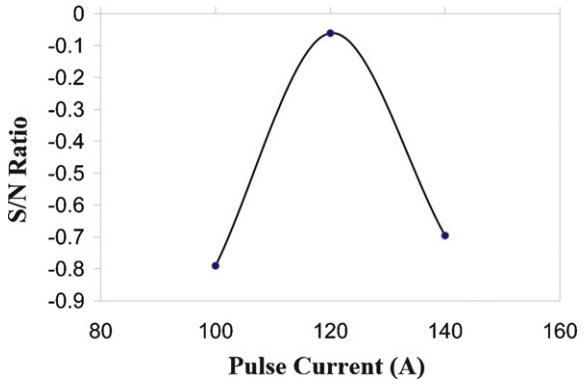

Fig. 3. Effect of pulse current on S/N ratio.

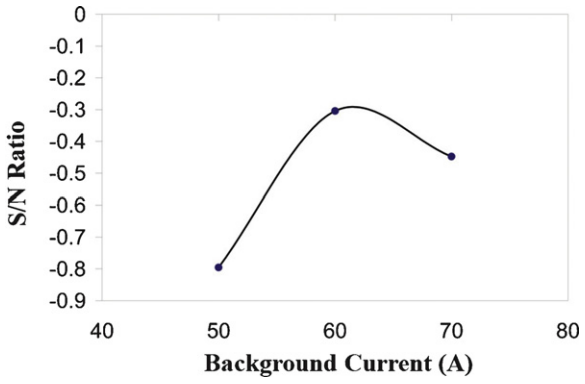

Fig. 4. Effect of background current on S/N ratio.

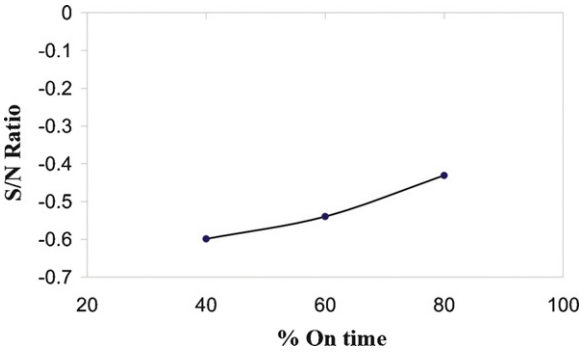

Fig. 5. Effect of % on time on S/N ratio.

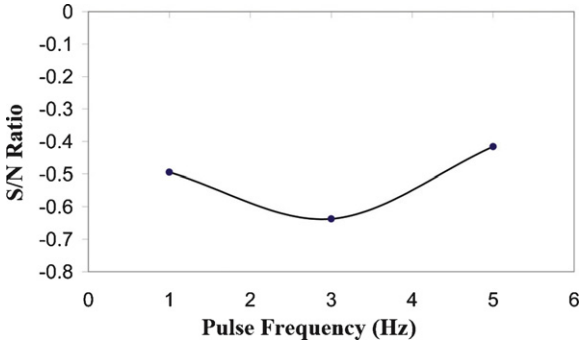

Fig. 6. Effect of pulse frequency on S/N ratio.

Table 5
The response table for S/N ratio.

Level	Factors			
	A	B	C	D
1	−0.790678	−0.795704	−0.577118	−0.494648
2	**−0.061100**	**−0.304342**	−0.539717	−0.637307
3	−0.696023	−0.447754	**−0.430966**	**−0.415845**

The optimum levels of the factors are given in bold (the highest value in the column)..

background current are more significant, while, pulse frequency and % on time are insignificant.

The response of the S/N ratio to pulse current is shown in Fig. 3. The mean S/N ratio goes up until it reaches a peak at the pulse current of 120 A. In fact, the pulse current of maximum corrosion resistance was observed at 120 A, which is the medium pulse current value among the three levels tested in this study. Thereafter, the mean S/N ratio decreases with increase of pulse current. This may result from the precipitate of the sigma and Cr_2N phases. On the other hand, the austenite and sigma contents have a key role on the corrosion resistance.

Fig. 7 represents the microstructure of weld metal at different conditions (a) at trial no. 1, in which the lowest pitting potential (0.88 V) was observed, (b) at trial no. 9 in which the intermediate pitting potential (0.93 V) was observed and (c) at trial no. 5 in which the highest pitting potential (1.03 V) was observed.

As seen in Fig. 7(a), the microstructure is characterized by nitrides precipitated in the ferrite phase. The ferrite content was 68% in this sample. The high ferrite content in Fig. 7(a) is due to the low heat input (0.630 kJ/mm) and rapid solidification under these conditions that impedes nitrogen migration to austenite. If the ferrite content is high, such as in weld metal under rapid cooling conditions, an intense nitride precipitation reaction occurs upon cooling since the solubility limit of the ferrite is exceeded and the nitrogen has insufficient time to partition to the austenite. In most cases these nitrides are Cr-rich and are thought to be primarily Cr_2N. The EDX analysis showed that the content of chromium in Cr_2N reached up to 75.3 wt.%. The high ferrite content (68%) and the Cr_2N precipitation decrease the corrosion resistance [20]. In addition, Cr_2N particles are also believed to be nucleation sites for pitting [21].

As shown in Fig. 7(b), it is clearly the presence of sigma phase at the ferrite–austenite interfaces, which are considered as preferential nucleation sites for the heterogeneous precipitation of intermetallic compounds. The formation of sigma phase in super duplex stainless steels is described by the decomposition of ferrite through an eutectoid transformation. The preferential precipitation of sigma phase from ferrite is due to the richness of chromium and molybdenum elements in the ferrite [22]. The sigma precipitation is confirmed by the EDX analysis of the white region in Fig. 7(b), as illustrated in Table 6, which is the result of high heat input (0.890 kJ/mm) and slow cooling rate under these conditions. On the other hand, the time of ferrite to austenite transformation was sufficient to acquiring the high austenite content that is approximately 45%. Also the sigma content was 26% in this sample. Since the sigma phase is believed to be nucleation site for pitting, hence σ

Table 6
Chemical composition of sigma and matrix phases determined by EDX analysis (wt.%).

Phase	Element			
	Chromium	Molybdenum	Nickel	Iron
γ	25.36	3.29	8.64	62.71
α	27.86	4.72	5.81	61.61
σ	32.62	9.51	5.36	52.51

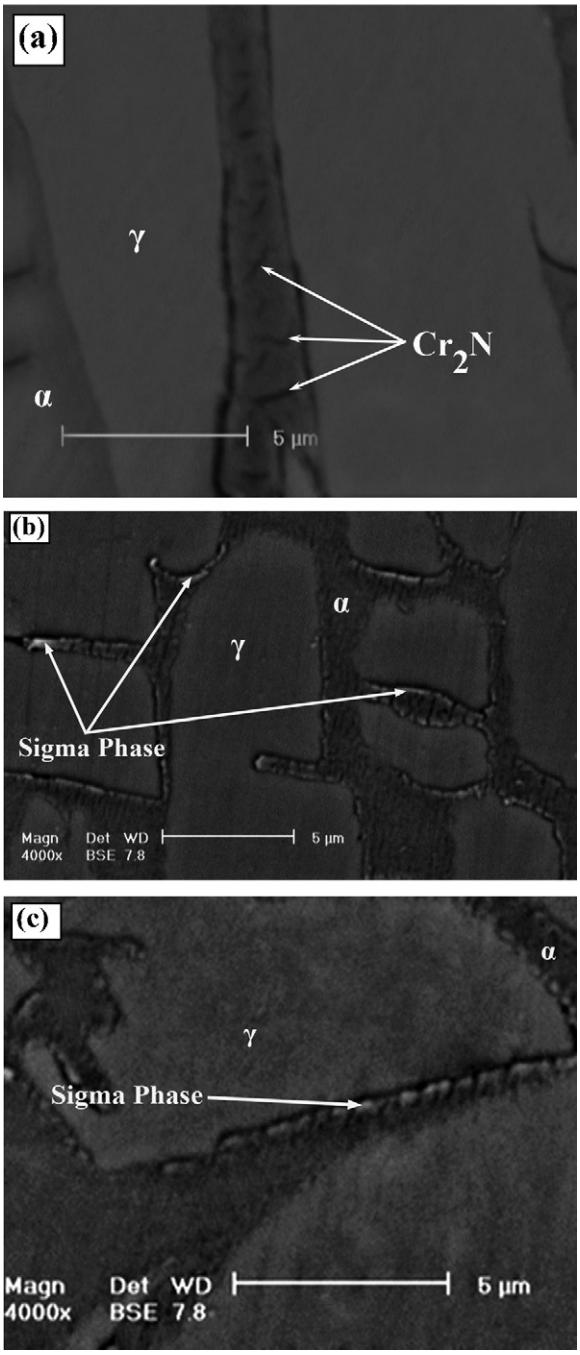

Fig. 7. SEM micrographs of UNS S32760 samples welded at different conditions: (a) trial no.1, (b) trial no.9 and (c) trial no.5.

phase precipitation promotes a decrease in the corrosion resistance of duplex and super duplex stainless steels [23].

As seen in Fig. 7(c), the microstructure is characterized by slightly sigma precipitated in the γ/α interfaces. The austenite and sigma content of this sample are measured to be about 43% and 7.8%, respectively, which is the result of intermediate heat input (0.756 kJ/mm) and cooling rate under these conditions. In fact, in these conditions the cooling rate is slow enough for adequate austenite formation (43% γ), but fast enough to reduce sigma precipitation (7.8% σ). This austenite content is very close to ideal value (50% γ). The high austenite content and low sigma precipitation in this sample, resulting in high corrosion resistance.

Table 7
Optimum working conditions.

Serial no.	Factors	Level	Values
1	Pulse current (A)	2	120
2	Background current (A)	2	60
3	% On time	3	80
4	Pulse frequency (Hz)	3	5

The response of the S/N ratio to the background current, Fig. 4, is similar to that for the pulse current. The mean S/N ratio increases at first as the background current increases from 50 to 60 A. The background current of maximum corrosion resistance was observed at 60 A, which is the medium background current value among the three levels tested in this study. The S/N ratio then decreases as the background current, increases to 70 A. The intermetallic precipitations and the austenite content in super duplex stainless steels affect the corrosion properties in a rather extensive way. Precipitation of brittle phases leads to a rapid reduction of the corrosion resistance; this is in agreement with the result of Pohl et al. [24] in a duplex stainless steel and Moura et al. [20] in a duplex stainless steel UNS S31803.

Fig. 5 shows response of the S/N ratio to the % on time. It can be seen from figure, % on time is insignificant. The slopes of the lines between 40–60 and 60–80 are almost the same. The mean S/N ratio increases linearly with % on time. So, the highest corrosion resistance was occurred at highest % on time (80). This may be due to the direct effect of % on time on the formation of austenite. An increasing of % on time was increased austenite content. The best corrosion properties are obtained with approximately equal amounts of austenite and ferrite [1]. It can be speculated from above discussions that the austenite and ferrite contents are functions of pulse current, background current and % on time.

Fig. 6 shows the response of the S/N ratio to pulse frequency. It can be seen from Fig. 6 that the mean S/N ratio drops to the bottom of the curve as the pulse frequency increases to 3 Hz (level 2) from 1 Hz (level 1). When the pulse frequency keeps increasing to 5 Hz (level 3), the mean S/N ratio bounces back upward and further rises to the highest value. Pulse frequency is the number of peak current pulses, which occur in one second of time and it is given by the inverse of the cycle time, T in seconds. A pulse cycle time (T) is defined as the period from the start of a pulse to the end of the background time just before the next pulse [25]. The observation on the response of the S/N ratio to pulse frequency may be mainly due to the fine or coarse grain structure [26]. However, detailed mechanisms dictating the response of the S/N ratio to pulse frequency need to be further investigated.

The Taguchi method can be employed to obtain the optimal level/factor combination of PCGTAW parameters. The Taguchi method uses the signal–noise to represent the quality characteristic, and the largest S/N ratio is requested. Table 4 shows the S/N ratios obtained using the Taguchi method, while Table 5 lists the responses for the S/N ratios. In Table 5, A2, B2, C3, and D3 illustrate the largest values of S/N ratios for factors A, B, C, and D, respectively. Consequently, A2B2C3D3 is the condition for the optimal parameter combination of the PCGTAW. Restated, the pulse current is 120 A, background current is 60 A, %on time is 80, and pulse frequency is 5 Hz, as presented in Table 7.

4.2. Analysis of variance (ANOVA) results

Analysis of the variance was used to determine the influence and relative importance of the different factors. The sum of the square (SS), the degree of freedom (D), the variance (V), and the percentage of the contribution to the total variation (P) are four parameters symbols typically used in ANOVA, which can be calculated as fol-

Table 8
Results of the ANOVA for corrosion resistance.

Symbol	Factors	Degree of freedom (D)	Sum of squares (SS)	Variance (V)	Corrected sums of squares (SS′)	Contribution (P, %)	Rank
A	Pulse current	2	0.0114000	0.0057000	0.0114000	66.28	1
B	Background current	2	0.0044667	0.0022333	0.0044667	25.97	2
C	% On time	2	0.0004667	0.0002333	0.0004667	2.71	4
D	Pulse frequency	2	0.0008667	0.0004333	0.0008667	5.04	3
Error		0	0	0	0	0	
Total		8	0.0172000			100	

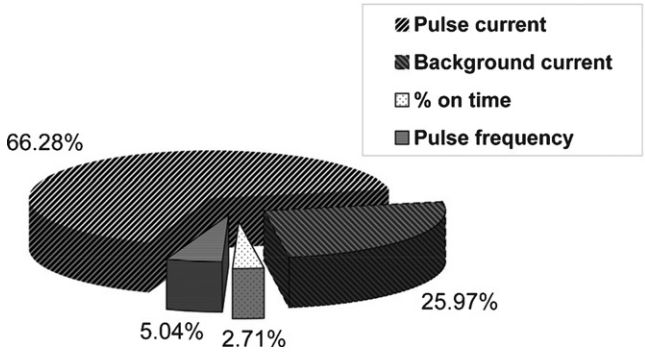

Fig. 8. Contribution of each factor on the performance statistics (Influential effects based on percentage distributions).

lowing equations (Eqs. (4)–(8)) [27]:

$$SS_T = \sum_i^m \eta_i^2 - \frac{1}{m}\left[\sum_{i=1}^m \eta_i\right]^2 \quad (4)$$

where SS_T is the total sum of squares, m is the total number of the experiments, and η_i is the S/N ratio at the ith test.

$$SS_p = \sum_{j=1}^t \frac{(S_{\eta_j})^2}{t} - \frac{1}{m}\left(\sum_{i=1}^m \eta_i\right)^2 \quad (5)$$

where SS_p represents the sum of squares from the tested factors, p the one of the tested factors, j the level number of this specific factor p, t the repetition of each level of the factor p, and S_{η_j} the sum of the S/N ratio involving this factor and level j.

$$V_p(\%) = \frac{SS_p}{D_p} \times 100 \quad (6)$$

where V_p is the variance from the tested factors, and D_p is the degree of freedom for each factor.

$$SS'_p = SS_p - D_p V_e \quad (7)$$

where SS_p' represents the corrected sum of squares from the tested factors, and V_e the variance for the error.

$$P_p(\%) = \frac{SS'_p}{SS_T} \times 100 \quad (8)$$

where P_p is the percentage of the contribution to the total variation of each individual factor.

The analysis of variance (ANOVA) of the DOE method was conducted and the results are shown in Table 8. It was observed that pulse current was the most significant PCGTAW parameter due to its highest percentage contribution (calculated percent contribution, P = 66.28%) among the process parameters (Table 8). The second order effect was the background current (calculated percent contribution, P = 25.97%) and the next significant parameters for the PCGTAW in order of importance were pulse frequency (5.04%) > % on time (2.71%). Percent contributions of all parameters are presented in Fig. 8.

In the ANOVA analysis, if the percentage error (P_e) contribution to the total variance is lower than 15%, no important factor is missing in the experimental design [27]. As shown in Table 8, the percentage error (P_e) is 0%. This indicates that no significant factors are missing in the experimental design.

4.3. Confirmation test

In order to verify experimental conclusions, confirmation test was performed. The confirmation test results compare with the predicted performance [13]. The confirmation test was performed by setting the optimum conditions of the four factors as: 120 A for pulse current; 60 A for background current; 80 for % on time and 5 Hz for the pulse frequency.

The pitting potential was found to be 1.06 V_{SCE} in the confirmation test. The predicted S/N ratio using the optimal level of the design parameters can be calculated as [28,29]:

$$\left[\frac{S}{N}\right]_{predicted} = \left[\frac{S}{N}\right]_m + \sum_{i=1}^n \left(\left[\frac{S}{N}\right]_i - \left[\frac{S}{N}\right]_m\right) \quad (9)$$

where $[S/N]_m$ is the total mean S/N ratio, $[S/N]_i$ is the mean S/N ratio at the optimal level, and n is the number of the main design parameters that affect the quality characteristic. In the case of pitting potential, the value of $[S/N]_m$ calculated from Table 4 is −0.515934. Also, $[S/N]_i$ for A2, B2, C3 and D3 can be obtained from Table 5. The corresponding values are −0.061100, −0.304342, −0.430966 and −0.415845, respectively. By using these values, Eq. (9) can be written as $[S/N]_{predicted}$ = −0.515934 + [(−0.061100 + 0.515934) + (−0.304342 + 0.515934) + (−0.430966 + 0.515934) + (−0.415845 + 0.515934)]. Therefore, the predicted S/N ratio (0.335549) for pitting potential can be obtained and the corresponding estimated pitting potential can also be calculated by using Eq. (3). This means that the value of S/N ratio (0.335549) at optimal condition (A2B2C3D3) is substituted into Eq. (3), and then Eq. (3) can be expressed as $0.335549 = -10\log(1/y^2)$. Finally, the estimated pitting potential (1.04 V_{SCE}) can be obtained. The results are shown in Table 9. There is a good agreement between the predicted and experimental pitting potentials.

Fig. 9 shows a SEM micrograph of the welded sample from the confirmation run. No precipitation or intermetallic phases appear on the micrograph and the microstructure consists of only ferrite and austenite. Furthermore, the austenite content was 48%, which is very close to ideal value (50% austenite). The anodic polarization curves of the welded sample from the confirmation run and from the base metal are shown in Fig. 10. It can be seen from Fig. 10 that the pitting potential of the optimized welding is very close (1.06 V_{SCE}) to the base metal (1.1 V_{SCE}), which is the highest value obtained in the present study.

Table 9
Results of the confirmation test using the optimized conditions.

	Optimal control parameters	
	Prediction	Experimental
Level	$A_2B_2C_3D_3$	$A_2B_2C_3D_3$
Pitting potential (V_{SCE})	1.04	1.06

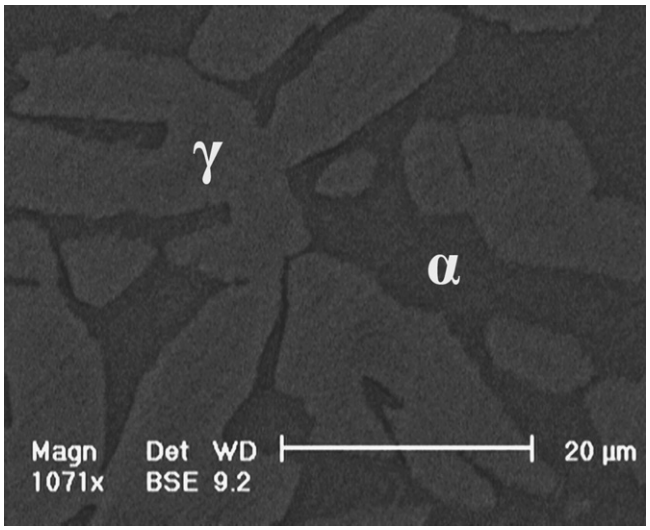

Fig. 9. SEM micrograph of the confirmation test using the optimized PCGTAW conditions.

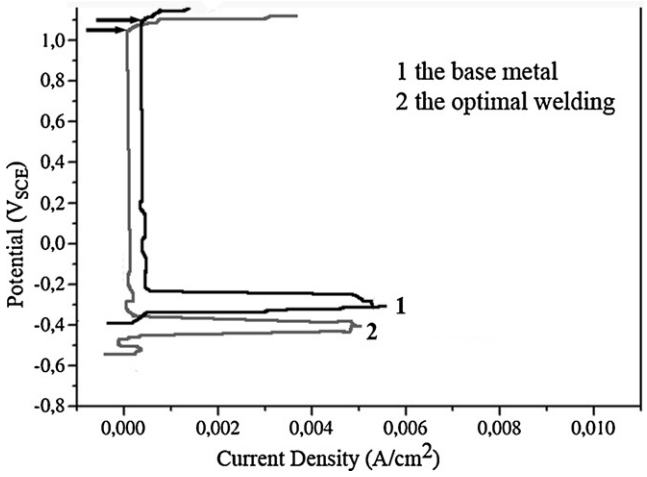

Fig. 10. Anodic polarization curves of the base metal and the optimal welding.

5. Conclusions

In this study, Taguchi design of experiment (L_9) was employed to optimize the effect of PCGTAW parameters on the corrosion resistance of super duplex stainless steel (UNS S32760) welds. The factors considered were pulse current, background current, % on time and pulse frequency. The higher-the-better S/N ratio was used to analyze the results of experiments. The conclusions drawn from this study are summarized as follows:

- Among the four factors and three levels tested, it was concluded that the pulse current had the most significant effect on the pitting potential and the background current had the next most significant effect. The effects of pulse frequency and % on time are less important when compared to the other factors.
- The percentage contributions of the pulse current, the background current, % on time, and pulse frequency to the corrosion resistance are 66.28%, 25.97%, 2.71% and 5.04%, respectively.
- The optimum conditions within the selected parameter values were found as the second level of pulse current (120 A), second level of background current (60 A), third level of % on time (80%) and third level of pulse frequency (5 Hz).
- The confirmation test was carried out at optimum working conditions. Pitting potential was increased to 1.06 V_{SCE} by setting the control factors. Predicted (1.04 V_{SCE}) and observed (1.06 V_{SCE}) pitting potential values are close to each other, which are the highest values obtained in the present study.

Acknowledgements

The authors would like to express their gratitude to the staff members of the Materials Engineering Department of Isfahan University of Technology (IUT) for their cooperation during these experiments.

References

[1] V. Muthupandi, P. Bala Srinivasan, S.K. Seshadri, S. Sundaresan, Mater. Sci. Eng. A 358 (2003) 9–16.
[2] R.N. Gunn, Duplex Stainless Steels—Microstructure, Properties and Applications, Abington Publishing, Cambridge, 2003.
[3] K.M. Lee, H.S. Cho, D.C. Chjoi, J. Alloys Compd. 285 (1999) 156–161.
[4] D.Y. Kobayashi, S. Wolynec, Mater. Res. 2 (4) (1999) 239–247.
[5] J.C. Lippold, D.J. Kotecki, Welding Metallurgy and Weldability of Stainless Steels, John Wiley & Sons, New York, 2005.
[6] J.O. Nilsson, Mater. Sci. Technol. 8 (1992) 685–700.
[7] A.J. Ramirez, J.C. Lippold, S.D. Brandi, Metall. Mater. Trans. A 34 (2003) 1575–1597.
[8] S.S.M. Tavares, J.M. Pardal, L.D. Lima, I.N. Bastos, A.M. Nascimento, J.A. de Souza, Mater Charact. 58 (2007) 610–616.
[9] Practical guidelines for the fabrication of duplex stainless steels, International Molybdenum Association, London, 1999.
[10] T. Senthil Kumar, V. Balasubramanian, M.Y. Sanavullah, Mater. Des. 28 (2007) 2080–2092.
[11] A.A. Gokhale, D.J. Tzavaras, H.D. Brody, G.M. Ecer, Proceedings of conference on grain refinement in casting and welds, St. Louis (MO), TMS-AIME, 1982, pp. 223–247.
[12] P.K. Giridharan, N. Murugan, Int. J. Adv. Manuf. Technol. 40 (2009) 478–489.
[13] Z. Beril Gonder, Y. Kaya, I. Vergili, H. Barlas, Sep. Purif. Technol. 70 (2010) 265–273.
[14] Image Tool version 3.0, University of Texas Health Science Center at San Antonio, free software, available in http://ddsdx.uthscsa.edu/dig/itdesc.html (accessed on 09.03.2007).
[15] M.A. Domínguez-Aguilar, R.C. Newman, Corros. Sci. 48 (2006) 2560–2576.
[16] C.J. Park, H.S. Kwon, M.M. Lohrengel, Mater. Sci. Eng. A 372 (2004) 180–185.
[17] J.M. Pardal, S.S.M. Tavares, M. Cindra Fonseca, J.A. de Souza, R.R.A. Côrte, H.F.G. de Abreu, Mater. Charact. 60 (2009) 165–172.
[18] S. Madhav Phadke, Quality Engineering Using Robust Design, Prentice Hall, NJ, 1989.
[19] O. Tan, A. Sahin Zaimoglu, S. Hinislioglu, S. Altun, Taguchi approach for optimization of the bleeding on cement-based grouts, Tunnel. Undergr. Space Technol. 20 (2005) 167–173.
[20] V.S. Moura, L.D. Lima, J.M. Pardal, A.Y. Kina, R.R.A. Corte, S.S.M. Tavares, Mater. Charact. 59 (2008) 1127–1132.
[21] H.Y. Liou, R.I. Hsieh, W.T. Tsai, Mater. Chem. Phys. 74 (2002) 37–42.
[22] R. Badji, M. Bouabdallah, B. Bacroix, C. Kahloun, B. Belkessa, H. Maza, Mater. Charact. 59 (2008) 447–453.
[23] V.M. Linton, N.J. Laycock, S.J. Thomsen, A. Kumpers, Eng. Fail. Anal. 11 (2004) 243–256.
[24] M. Pohl, O. Storz, T. Glogowski, Mater. Charact. 58 (2007) 65–71.
[25] H. Tong, T. Ueyama, S. Harada, M. Ushio, Sci. Technol. Weld. Join. 6 (4) (2001) 203–208.
[26] A. Kumar, S. Sundarrajan, J. Mater. Des. 30 (4) (2009) 1288–1297.
[27] Y. Ma, H. Hu, D. Northwood, X. Nie, J. Mater. Process. Technol. 182 (2007) 58–64.
[28] R. Roy, A Primer on the Taguchi Method, Van Nostrand Reinhold, New York, 1990.
[29] K.D. Kim, D.N. Han, H.T. Kim, Chem. Eng. J. 104 (2004) 55–61.